Wrinkling of a normally loaded, spinning, elastic membrane: an asymptotic approximation

Ciprian D. Coman[1†]

[1]*School of Computing & Engineering*,
University of Huddersfield, HD1 3DH, Huddersfield, UK

July 9, 2023

Abstract

This paper revisits recent work on the edge wrinkling experienced by spinning circular membranes loaded by a transverse uniform pressure. The corresponding stability analysis is carried out within the framework of the Föppl-von Kármán nonlinear plate theory. It is shown herein that the effect of rotation of the membrane is similar to an in-plane tension applied on its outer perimeter, an observation that proves to be quite effective in obtaining a tight upper bound for the critical wrinkling load of the problem. Comparisons between the simplified model and direct numerical simulations of the full eigenproblem provide further insight into the accuracy and limitations of the derived results.

Keywords: wrinkling, localised deformations, boundary layers, FvK plate theory, asymptotic methods

[†]cdc3p@yahoo.com

1 Introduction

Historically, most textbooks on linear elasticity have invariably included as a standard fixture a brief account of the classical problem of a spinning disc (or a thick hollow cylinder) which rotates with constant angular speed around a vertical axis passing through its centre (e.g., [1, 2, 3, 4, 5]). This scenario is usually employed to illustrate practical strategies for solving simple boundary-value problems that crop up in two-dimensional approximate theories such as plane stress (or plane strain). Notwithstanding the simplicity of the corresponding solution, the above configuration was at one time of great interest in the development of steam/gas turbines and rotating machineries (see [6, 7, 8] and the references therein).

Lamb and Southwell [9, 10] provided the first systematic investigations into the natural frequencies associated with the transverse vibrations of spinning discs; in particular, they established that these can be approximated quite accurately as a combination of terms arising separately from the centrifugal stresses of rotation and the bending stresses of the disc. Extensions to discs with different cross-sections and clamping geometries were later given by Prescott [3]; Simmonds [11] corrected some inaccurate conclusions in [10], while Eversman and Dodson [12] relied on suitable Frobenius series solutions to obtain accurate numerical values for the natural frequencies corresponding to a range of different boundary constraints. Renewed interest in the spinning disc configuration came in the early 1960's, with the advent of floppy disc magnetic recording devices (e.g., see [13, 14]). This problem is more complicated as it involves the interaction between the disc and a transverse load (the reading head) [15, 16, 19]; realistic modelling also requires some sort of coupling between the elastic deformation of the spinning disc and the fluid dynamics of the gas film beneath it (e.g., [17, 18, 20, 21, 22, 23]).

The presence of dynamic effects in the above problems raises some subtle questions regarding the appropriate choice of plate equations. The original works [9, 10] were based on an ad hoc extension of the classical Kirchhoff plate theory; more specifically, it was assumed *a priori* that the in-plane stresses due to the centrifugal forces influenced the bending response, but the latter had no effect on the former. Nowinski [24] proposed a rational modification of the Föppl-von Kármán (FvK) nonlinear plate theory that incorporates the aforementioned centrifugal effect through a modification of the usual Airy stress function. In more recent times, Baddour and Zu [25] suggested an "improved" set of three coupled fully nonlinear plate equations, with rotary inertia being included as well. Some of the claims made by these authors were at odds with experimental evidence available for rotating elastic discs. Chen [26] showed that, by adopting a consistent asymptotic simplification of the equations found in [25], one can recover both the linearised version used in [9, 10] and Nowinski's nonlinear form [24], while the usefulness of the "improved" terms is in general questionable without additional qualifying remarks.

In an interesting paper motivated by aerospace applications (e.g., solar sails), Delapierre *et al.* [27] have recently considered the wrinkling of a spinning circular "membrane" loaded by a uniform transverse pressure. Their study dealt essentially with a thin elastic plate (rather than a pure membrane) as the bending stiffness was included in the model; centrifugal forces were also accounted for by adopting Nowinski's [24] modification of the FvK equations already mentioned above (see also, [38]). The approach taken by the authors of [27] was largely based on experiments and brute-force numerical simulations of the corresponding eigenproblem. They found that the eigenmodes of the spinning plate have the tendency to concentrate around its outer rim as the angular speed increases, a phenomenon that is loosely reminiscent of Rayleigh's whispering-gallery modes [28, 29] (see also [30]); Figure 1 shows contour plots of the transverse displacement buckling modes for three different rotational speeds. It is one of the main goals of the present paper to shed further light on the scenario studied in [27], by approaching it through the lens of asymptotic theory. More specifically, we intend

to establish a connection between the origin of the localised eigendeformations reported therein and a much broader class of problems involving normally loaded circular thin elastic plates. Numerical

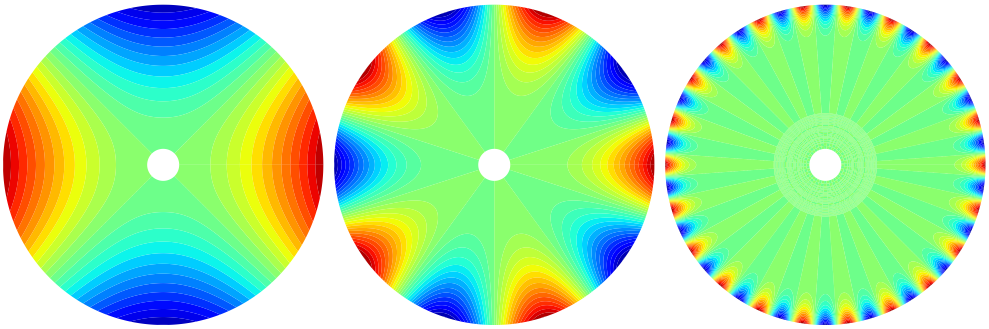

Figure 1: Localised transverse displacement eigenmodes in the normally loaded spinning annular plate considered in [27]; the angular speed increases from left to right.

solutions together with a detailed chronology of the key research regarding this particular configuration appeared in [31], while further theoretical aspects were explored in [32, 33, 34, 35, 36]. Broadly speaking, in all of these investigations it was found that the radially symmetric nonlinear solution of the FvK thin-plate theory leads to the appearance of compressive azimuthal stresses near the outer rim of the plate, hence the local character of the corresponding buckling patterns. For an additional uniform in-plane tension applied to the outer perimeter of the plate the out-of-plane deformations turned out to be confined within a narrow boundary-layer adjacent to that location, provided that the tensile forces were sufficiently strong. But it must be stressed that the local nature of the linear bifurcation modes prevails even in the absence of this external tension (e.g., see [31, 32, 37]). In light of these observations, we remark that the wrinkling studied by Delapierre *et al.* [27] can be largely traced back to the transverse load present in their model, with the rotation of the disc being only partly responsible for introducing a radial in-plane tension (i.e., a stiffening of the disc).

We commence our study in the next section with a brief overview of the key equations for the bifurcation problem governing the linear instabilities of the normally loaded spinning disc. One of the aims of that section is to show that the corresponding stability scenario considered in [27] can be conveniently cast within the general framework proposed in our earlier related investigations [33, 35, 36]. The qualitative similarities and differences between the new configuration and our previous studies are illustrated further in §3, which contains a selection of representative numerical results that complement those already available in the literature. Guided in part by this new information, we then suggest several asymptotic simplifications which are fully developed in §4. Further comparisons between the predictions of the (approximate) reduced model and the corresponding direct numerical simulations of the original stability problem confirm the validity/accuracy of the results derived therein. The paper concludes with a general discussion of our results and some remarks for possible future extensions.

2 The key equations

A brief account of the key differential equations and assumptions used in the rest of the paper is presented in this section. This mathematical model was discussed from a purely numerical perspective in reference [27], to which interested readers are referred for an alternative presentation. Here, we will be content with just a few highlights required to set the stage and make the paper reasonably self-contained.

The situation of interest in the reference just mentioned above concerned an annular thin elastic disc, spinning about its vertical axis of symmetry with constant angular speed ω; an additional transverse pressure p was also supposed to act upon the lateral surface of the annulus (see Figure 2). The question of interest was to identify the critical value of p for which the disc buckles. This scenario is closely related to our earlier work [31, 32, 33, 35, 36] which dealt with the (static) case of a full circular plate subjected to either a transverse pressure or a point load. In those studies we established a fairly detailed description of the asymptotic structure for the edge-buckling phenomenon observed in all of the scenarios investigated. For now we will postpone a more in-depth comparison of that body of work with [27], but we will return to this aspect later in §5.

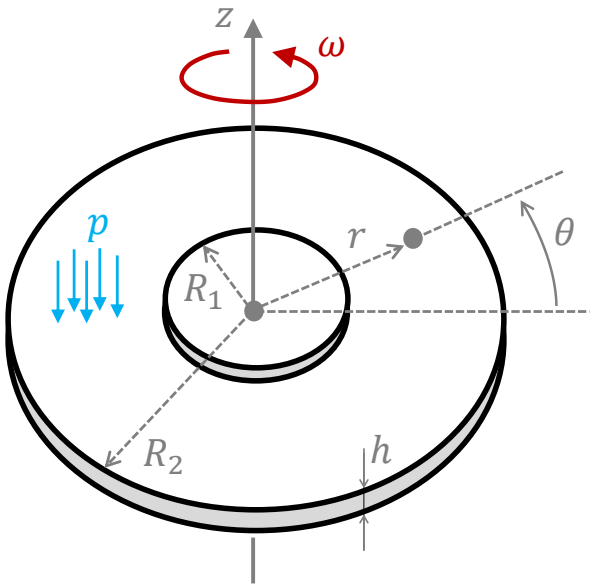

Figure 2: The geometry of the spinning annular disc considered in the main text; its mid-surface is parametrised by the polar coordinates (r, θ) with $R_1 \leq r \leq R_2$ and $0 \leq \theta < 2\pi$. A uniform transverse pressure p acts upon the lateral surface of the disc.

The annular geometry of the disc is characterised by an inner radius R_1, outer radius R_2, and thickness h (with $h/R_2 \ll 1$). Linear elasticity is assumed for the constitutive behaviour of the plate material, with E being its Young's modules and ν the corresponding Poisson's ratio; ρ_m denotes the mass density of the plate. We define a cylindrical coordinate system (r, θ, z) that rotates with the disc, with the z-axis coincident with the disc's symmetry axis. In this reference frame the inertial force is indistinguishable from a body force; the associated plane stress stress problem is easily solved within the context of linear elasticity and can be found in most textbooks on the subject (e.g., see [1, 2, 3, 4]). Since in the present scenario the applied transverse pressure is responsible for moderate coupling between bending and stretching in the plate mid-plane, this plane-stress solution is not applicable here. Nowinski [24] has provided a convenient modification of the usual Föppl-von Kármán (FvK) plate theory that takes into account the spinning feature mentioned above; a detailed derivation of the equations is also included in Nayfeh's book [38]. Within that framework the components of the membrane stress tensor require the solution of a set of nonlinear differential equations which are outlined next.

All theoretical developments contained in this paper are based on the modified version of the classical FvK approximation (e.g., [39, 40, 41]), written in terms of the plate transverse displacement $w \equiv w(r,\theta,t)$ and an Airy-type stress function $f \equiv f(r,\theta,t)$; the rotating coordinate system is the same as already explained above. These equations assume the well-known form [24, 38]

$$\begin{cases} \rho_m h\dfrac{\partial^2 w}{\partial t^2} + D\nabla^4 w + \underline{\rho_m h\omega^2\left(\dfrac{1}{2}r^2\nabla^2 w + r\dfrac{\partial w}{\partial r}\right)} - [f,w] = p\,, \\[2ex] \nabla^4 f + \dfrac{Eh}{2}[w,w] - \underline{2\rho_m h(1-\nu)\omega^2} = 0\,, \end{cases} \tag{2.1}$$

where $D \equiv Eh^3/12(1-\nu^2)$ is the bending rigidity of the plate and the bracket represents the Monge-Ampère operator defined by

$$[g_1,g_2] := (\nabla^2 g_1)(\nabla^2 g_2) - (\boldsymbol{\nabla}\otimes\boldsymbol{\nabla} g_1) : (\boldsymbol{\nabla}\otimes\boldsymbol{\nabla} g_2)\,,$$

for any two smooth functions g_1 and g_2. The stress function is related to the membrane stress tensor $\boldsymbol{N}$ according to

$$\boldsymbol{N} = \left(\nabla^2 f - \underline{\frac{1}{2}\rho_m h\omega^2 r^2}\right)\boldsymbol{I}_2 - \boldsymbol{\nabla}\otimes\boldsymbol{\nabla} f\,, \tag{2.2}$$

with $\boldsymbol{I}_2$ being the usual two-dimensional identity tensor; all of the above symbols/notations are the standard ones (e.g., see Chapter 1 in [42]). We note in passing that the underlined terms in (2.1) and (2.2) are not present for the non-spinning case of a circular plate.

It is useful to re-scale (2.1) by introducing the non-dimensional quantities

$$\rho := \frac{r}{R_2}\,, \qquad \eta := \frac{R_1}{R_2}\,, \qquad \Omega := \omega R_2^2\left(\frac{\rho_m h}{D}\right)^{1/2}, \qquad \tau := R_2^{-2}\left(\frac{D}{\rho_m h}\right)^{1/2} t\,, \tag{2.3a}$$

$$\widehat{w} := \left[12(1-\nu^2)\right]^{1/2}\left(\frac{w}{h}\right), \qquad \widehat{f} := \frac{f}{D}\,, \qquad \Lambda_{\rm v} := \left[12(1-\nu^2)\right]^{3/2}\left(\frac{R_2}{h}\right)^4\left(\frac{p}{E}\right), \tag{2.3b}$$

which leads to the simplified form of the above system,

$$\frac{\partial^2\widehat{w}}{\partial\tau^2} + \nabla_*^4\widehat{w} + \Omega^2\left(\frac{1}{2}\rho^2\nabla_*^2\widehat{w} + \rho\frac{\partial\widehat{w}}{\partial\rho}\right) - [\widehat{w},\widehat{f}] = \Lambda_{\rm v}\,, \tag{2.4a}$$

$$\nabla_*^4\widehat{f} + \frac{1}{2}[\widehat{w},\widehat{w}] - 2(1-\nu)\Omega^2 = 0\,, \tag{2.4b}$$

where

$$\nabla_*^2 \equiv \frac{\partial^2}{\partial\rho^2} + \frac{1}{\rho}\frac{\partial}{\partial\rho} + \frac{1}{\rho^2}\frac{\partial^2}{\partial\theta^2} \qquad \text{and} \qquad \nabla_*^4 = \nabla_*^2\nabla_*^2\,;$$

these equations are subject to the boundary conditions recorded in Appendix A. Note that the re-scaled radial range is now $\eta \le \rho \le 1$; the case $0 < \eta \ll 1$ will be excluded from the analysis included in what follows.

Before we can deal with the formulation of the wrinkling problem itself, it is necessary to examine the nonlinear *axisymmetric* basic state. By letting $\widehat{w} =: \mathring{w}(\rho)$ and $\widehat{f} =: \mathring{f}(\rho)$ it can be shown that (2.4) are reduced to

$$\mathcal{L}_0[\Theta] - \frac{\Theta\Phi}{\rho} = \frac{\Lambda_{\rm v}}{2\rho}(\rho^2-1)\,, \qquad \mathcal{L}_0[\Phi] + \frac{\Theta^2}{2\rho} = -(\nu+3)\Omega^2\rho\,, \tag{2.5}$$

where

$$\Theta \equiv \Theta(\rho;\Lambda,\Omega) := \frac{d\mathring{w}}{d\rho}\,, \qquad \Phi \equiv \Phi(\rho;\Lambda,\Omega) := \frac{d\mathring{f}}{d\rho} - \frac{1}{2}\Omega^2\rho^3\,, \tag{2.6}$$

and

$$\mathcal{L}_0 := \frac{d^2}{d\rho^2} + \frac{1}{\rho}\frac{d}{d\rho} - \frac{1}{\rho^2}\,.$$

Equations (2.5) must be solved subject to an appropriate set of boundary conditions obtained from those recorded in Appendix A; these edge constraints are stated below for easy reference

$$\Theta(\eta) = 0\,, \qquad \frac{d\Phi}{d\rho}(\eta) - \left(\frac{\nu}{\eta}\right)\Phi(\eta) = -\Omega^2\eta^2\,, \tag{2.7a}$$

$$\frac{d\Theta}{d\rho}(1) + \nu\Theta(1) = 0\,, \qquad \Phi(1) = 0\,. \tag{2.7b}$$

Potential bifurcations from the radially symmetric (time-independent) solution outlined above can be easily explored by considering perturbations of the form $\widehat{w}(\rho,\theta,\tau) \to \mathring{w}(\rho) + \widehat{w}(\rho,\theta,\tau)$ and $\widehat{f}(\rho,\theta,\tau) \to \mathring{f}(\rho) + \widehat{f}(\rho,\theta,\tau)$, which are then substituted into (2.4) followed by the usual linearisation of the resulting expressions. The outcome of these manipulations can be shown to be

$$\begin{cases} \dfrac{\partial^2\widehat{w}}{\partial\tau^2} + \nabla_*^4\widehat{w} + \Omega^2\left(\dfrac{1}{2}\rho^2\nabla_*^2\widehat{w} + \rho\dfrac{\partial\widehat{w}}{\partial\rho}\right) - [\widehat{w},\mathring{f}] - [\widehat{f},\mathring{w}] = 0\,, & \text{(2.8a)} \\[2ex] \nabla_*^4\widehat{f} + [\widehat{w},\mathring{w}] = 0\,. & \text{(2.8b)} \end{cases}$$

One possible attack strategy for the bifurcation system (2.8) is to consider separable-variable functions of the form

$$\big(\widehat{w}(\rho,\theta,\tau),\widehat{f}(\rho,\theta,\tau)\big) = \big(W(\rho),F(\rho)\big)\exp\big[\mathrm{i}(m\theta + s\tau)\big]\,, \qquad m = 0,1,2\ldots\,, \tag{2.9}$$

for some $s \in \mathbb{C}$ ($\mathrm{i} = \sqrt{-1}$). When substituted back into the two equations above this leads to the elimination of both the azimuthal coordinate and the second-order time-derivative in (2.8a). More specifically, the parameter $s^2 =: \lambda$ will play the role of an eigenvalue, and it should be also clear that $\lambda = \lambda(\Lambda_{\mathrm{v}};\Omega,m)$. In the present context (e.g., see [27]) the common approach employed in the literature for identifying the critical buckling pressure of the spinning disk, $\Lambda_{\mathrm{v}}^{(c)}$ (say), would be to fix Ω and then look for those values of $\Lambda_{\mathrm{v}} = \Lambda_{\mathrm{v}}^{(m)}$ (for each $m = 0,1,2,\ldots$) such that $\lambda(\Lambda_{\mathrm{v}}^{(m)};\Omega,m) = 0$; the global minimum of this discrete set of values represents the desired *critical load*, i.e.

$$\Lambda_{\mathrm{v}}^{(c)} := \min\big\{\Lambda_{\mathrm{v}}^{(m)} \;\big|\; m = 0,1,2,\ldots\big\}\,. \tag{2.10}$$

The unique m-value for which the minimum in (2.10) is attained represents the so-called *critical mode number*, and corresponds to the number of eigenmodal half-"waves" around the azimuthal span of the annular domain; such a quantity will be identified as m_c in what follows. This approach provides the determination of the main parameter of interest (i.e., Λ_{v} – see its definition in (2.3)) in a rather indirect way which, while acceptable from a numerical point of view, does obscure the asymptotic structure we are looking for. Hence, here we will follow an alternative route that is more straightforward and avoids the additional numerical overhead involved in the strategy outlined above. As our buckling problem is conservative, we can identify the critical load $\Lambda_{\mathrm{v}}^{(c)}$ from a pseudo-static approach, by setting $s = 0$ in (2.9) right from the outset and discarding the time-derivative term in (2.8a). The upshot is that

by doing so we end up with a (static) generalised eigenvalue problem in $\Lambda_{\rm v}$, which has several points in common with our previous work (e.g., see [32, 35, 36]).

Performing the requisite calculations it turns out that the unknown radial amplitudes in (2.9) satisfy a linear system of two coupled ordinary differential equations

$$\mathcal{L}_{11}[W] + \mathcal{L}_{12}[F] = 0\,, \qquad \mathcal{L}_{21}[W] + \mathcal{L}_{22}[F] = 0\,, \tag{2.11}$$

where

$$\mathcal{L}_{ij} \equiv \begin{cases} \displaystyle\sum_{k=0}^{4} \mathcal{A}_{ijk} \frac{d^k}{d\rho^k}\,, & \text{if } (i,j) = (1,1) \text{ or } (i,j) = (2,2)\,, \\[2ex] \displaystyle\sum_{k=0}^{2} \mathcal{A}_{ijk} \frac{d^k}{d\rho^k}\,, & \text{if } (i,j) = (1,2) \text{ or } (i,j) = (2,1)\,, \end{cases}$$

with the definitions of the coefficients $\mathcal{A}_{ijk}$ being relegated to Appendix B. The equations (2.11) are to be solved subject to an appropriate set of boundary conditions (easily obtained from the formulae recorded in Appendix A); at the inner rim of the plate (at $\rho = \eta$),

$$W = \frac{dW}{d\rho} = 0\,, \tag{2.12a}$$

$$\frac{d^2F}{d\rho^2} - \left(\frac{\nu}{\rho}\right)\frac{dF}{d\rho} + \left(\frac{\nu m^2}{\rho^2}\right)F = 0\,, \tag{2.12b}$$

$$\frac{d^3F}{d\rho^3} + \left(\frac{1}{\rho}\right)\frac{d^2F}{d\rho^2} - \frac{1}{\rho^2}\big[1 + (2+\nu)m^2\big]\frac{dF}{d\rho} + \frac{1}{\rho^3}\big[(3+\nu)m^2\big]F = 0\,, \tag{2.12c}$$

while for the stress-free outer edge (at $\rho = 1$)

$$F = \frac{dF}{d\rho} = 0\,, \tag{2.13a}$$

$$\frac{d^2W}{d\rho^2} + \nu\frac{dW}{d\rho} - \nu m^2 W = 0\,, \tag{2.13b}$$

$$\frac{d^3W}{d\rho^3} + \frac{d^2W}{d\rho^2} - \big[1 + (2-\nu)m^2\big]\frac{dW}{d\rho} + \big[(3-\nu)m^2\big]W = 0\,. \tag{2.13c}$$

In order to gain insight into the structure that underpins our bifurcation system (2.11) together with the boundary conditions (2.12) and (2.13), we now turn to some direct numerical simulations of these equations. All numerical work reported in the next section was carried out by using standard routines available in MATLAB.

3 Numerical results

As already mentioned, our numerical strategy for solving the wrinkling problem discussed earlier is rather different from the route taken in [27]. We recall that for a given Ω, the corresponding equations will be solved by treating the mode number $m > 0$ as a continuous variable; the critical load values ($\Lambda_{\rm v}^{(c)}$) and mode numbers (m_c) will then be obtained by numerically minimising $\Lambda_{\rm v} = \Lambda_{\rm v}(m)$. A

preliminary check of this approach was done by calculating the aforementioned critical values for $\Omega = 64$ and $\Omega = 200$ – the only Ω's for which explicit information is given in [27]. Our computed values were found to be identical to those previously reported, hence confirming that our equations in §2 are indeed equivalent to the formulation given in [27].

Before discussing our small sample of numerical solutions, we remark that the coefficients of the bifurcation system (2.11) depend on the pre-buckling stresses $\mathring{N}_{rr}$ and $\mathring{N}_{\theta\theta}$ (see Appendix B), rather than on the quantities Φ and Θ that feature in equations (2.5). In the interest of brevity, we will concentrate our attention only on the former quantities.

Examples of critical eigenmodes of the full wrinkling problem set up in §2 are shown in Figure 3 for a selection of increasing angular speeds Ω (mentioned in the caption). These results correspond to $\eta = 0.1$ and $\nu = 1/3$, while in Figure 4 we include similar information for $\eta = 0.5$. It is noted here that the transverse deflection W has a similar shape to that seen in the in-plane bending of a radially stretched sectorial plate [43], but this similarity is only visual as a more detailed mathematical investigation will confirm shortly. As η increases from 0.1 to 0.5, the effect of localisation is weakened; it is clear that the W-mode for $\Omega = 100$ when $\eta = 0.5$ extends over almost the entire breadth of the annular domain and can hardly be regarded as being truly localised. The stress function F behaves in a similar fashion to W, but owing to the boundary condition (2.13a) this function has to vanish on the outer rim of the plate. We note that as Ω grows, and the localised behaviour becomes progressively more accentuated, the W-modes increase in magnitude, but for the the F-modes exactly the opposite is true.

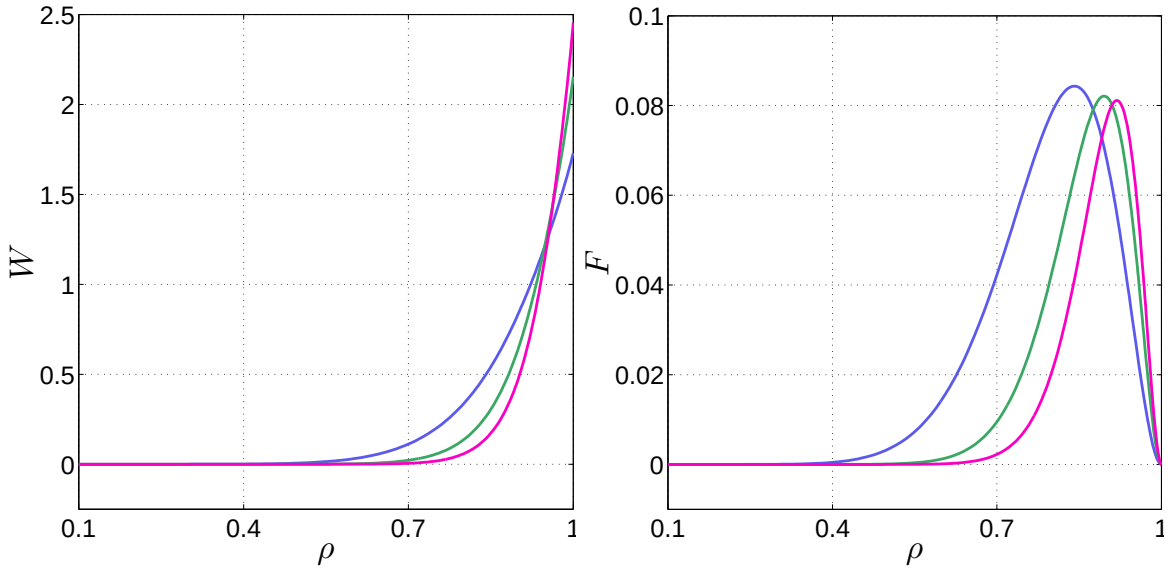

Figure 3: Sample of critical eigenmodes for $\eta = 0.1$: $\Omega = 100$ (blue), $\Omega = 200$ (green), and $\Omega = 300$ (magenta). In each figure, as Ω increases, the eigenfunctions move towards the outer edge of the plate ($\rho = 1$); all functions are normalised so that $\int_0^1 W^2(\rho)\,\mathrm{d}\rho = 0.2$.

Details of the in-plane (or membrane) pre-buckling stresses corresponding to the eigenmodes already shown are included in Figures 5 and 6. There is clear evidence that $\mathring{N}_{rr}$ exhibits a slow radial variation across the entire annular domain, but $\mathring{N}_{\theta\theta}$ varies quickly near the inner rim ($\rho = \eta$) to adjust to the clamping constraint – see the second equation in (2.7a). Since the eigenmodes are localised near $\rho = 1$, we anticipate that this region of fast variation for the azimuthal stresses is likely to play a passive role. It is interesting to note the changes in the curvatures of the functions recorded in

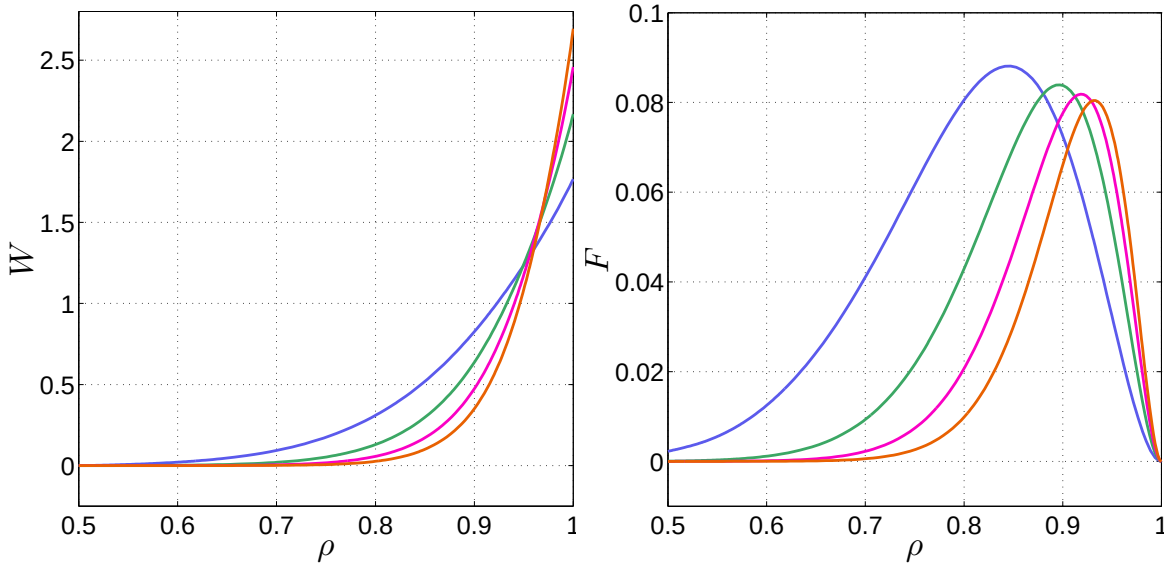

Figure 4: Sample of critical eigenmodes for $\eta = 0.5$: $\Omega = 100$ (blue), $\Omega = 200$ (green), $\Omega = 300$ (magenta), and $\Omega = 400$ (orange). The remarks mentioned in Fig. 3 apply here as well.

Figures 5 and 6; the pre-buckling stresses seen in the latter figure are almost "straight lines". From a mechanical point of view, the most important aspect vis-à-vis the basic state is the existence of possible compressive regions in the plate. As expected, the radial stresses are tensile throughout the plate, but their azimuthal counterparts accommodate both tensile and compressive regions, the latter being confined to a narrow ring-like zone adjacent to the outer edge of the annular configuration. It is clear from the information included in the right windows of Figures 5 and 6 that the extent of the compressive region shrinks (albeit slowly) as the angular speed Ω increases. In this sense, Ω plays a very similar role to the non-dimensional large parameter μ (the so-called "background tension") used in our related wrinkling studies [32, 33, 36].

4 Asymptotic simplifications

Informed by the numerical work outlined in the previous section, we now return to the relatively complicated system governing the edge-wrinkling scenario under consideration. The aim is to formulate a possible simplification strategy based on asymptotic arguments; our key assumption will be $\Omega \gg 1$ (which is to be understood in a broad sense). It is perhaps worth emphasising that our immediate concerns are not with unraveling the full asymptotic structure of the system (for that aspect see [49]).

Given the rather different nature of the two sets of equations involved, (2.5) and (2.11), respectively, it seems appropriate to consider them separately. We start in the next section with a few observations regarding the behaviour of the base state. These will then be amplified in §4.2, where a possible asymptotic approximation of the eigensystem (2.11)–(2.13) is fully fleshed out.

4.1 The basic state

It is a well-established fact that a thin plate subjected to a transverse uniform pressure can display a range of different behaviours, depending on the magnitude of the applied load (e.g., see [50, 51]). The

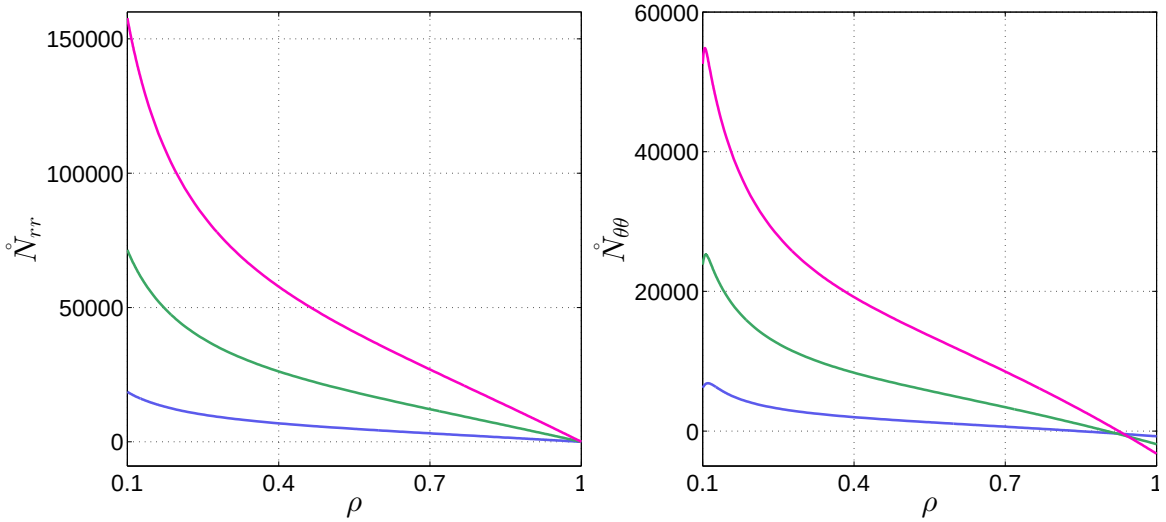

Figure 5: Axisymmetric membrane stress distribution at the onset of wrinkling for $\eta = 0.1$. The radial ($\mathring{N}_{rr}$) and azimuthal ($\mathring{N}_{\theta\theta}$) pre-buckling stresses are obtained from (B.1) and correspond to the eigenmodes of Fig. 3.

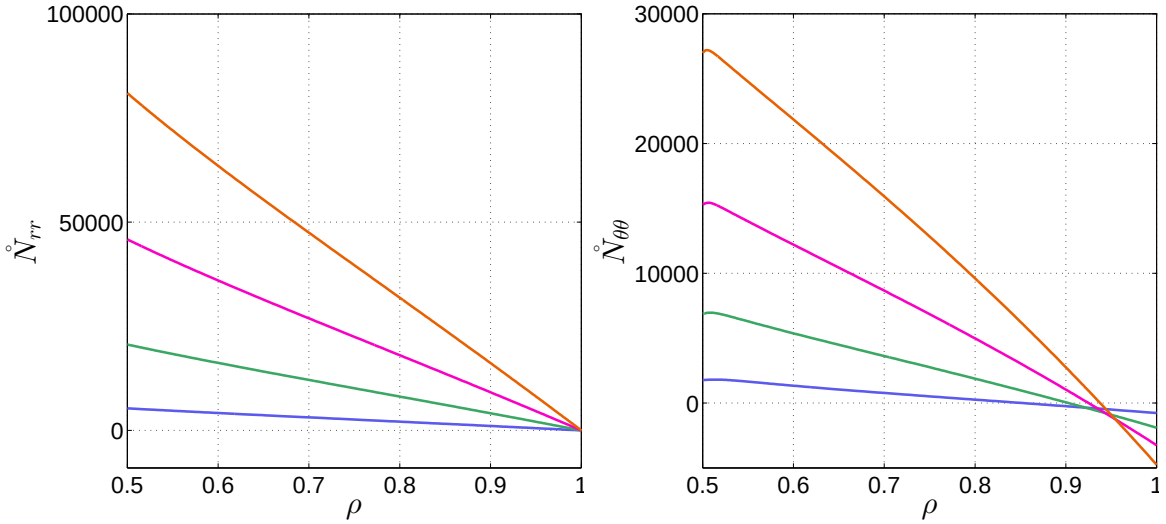

Figure 6: Same as per Fig. 5, except that here the pre-buckling stresses correspond to the eigenmodes included in Fig. 4 ($\eta = 0.5$).

numerical evidence included in [27] suggests that the onset of wrinkling in the spinning disc might be associated with *membrane-like* behaviour of the basic state if $\Omega \gg 1$. If this is true, then bending is expected to be confined only to narrow regions, stretching being the dominant effect across most of the spatial domain occupied by the plate. Similar findings were reported in our earlier works [31, 52, 53], within the context of several static wrinkling scenarios. We are thus prompted to consider an ad hoc simplification of the equations (2.5) by discarding the bending terms therein. A detailed comparison of the role played by the membrane and plate pre-buckling solutions on the edge-wrinkling of a uniformly pressurised circular thin film was performed in [32, 34], to which interested readers are referred for further details. In general, there is little loss of accuracy (and generality) by ignoring the bending stiffness in the pre-buckling range (e.g., [39]).

With this in mind we set

$$\Theta(\rho) = \Omega\Theta_0(\rho) + \dots \qquad \text{and} \qquad \Phi(\rho) = \Omega^2\Phi_0(\rho) + \dots\,, \tag{4.1}$$

thereby defining the rescaled pre-buckling fields Θ_0 and Φ_0; the dots stand for the usual higher-order terms that will not be needed in the present context. By writing

$$\Lambda_{\rm v} = \Omega^3\Lambda\,, \qquad \Lambda = \mathcal{O}(1)\,, \tag{4.2}$$

and then substituting (4.1) into (2.5), we find at leading order

$$\Theta_0\Phi_0 = \frac{1}{2}\Lambda(1-\rho^2)\,, \qquad \mathcal{L}_0[\Phi_0] + \frac{\Theta_0^2}{2\rho} = -(\nu+3)\rho\,. \tag{4.3}$$

Further elimination of Θ_0 in (4.3) then yields a non-dimensional version of the Hencky-Föppl equation (e.g., see [44]) for a pure membrane subjected to a transverse uniform pressure,

$$\mathcal{L}_0[\Phi_0] + \frac{\Lambda^2}{8\Phi_0^2}\left[\frac{(1-\rho^2)^2}{\rho}\right] + (\nu+3)\rho = 0\,. \tag{4.4}$$

This equation must be solved subject to the edge constraints

$$\frac{d\Phi_0}{d\rho}(\eta) - \left(\frac{\nu}{\eta}\right)\Phi_0(\eta) = -\eta^2 \qquad \text{and} \qquad \Phi_0(1) = 0\,. \tag{4.5}$$

The boundary-value problem (4.4)-(4.5) was investigated by Simmonds [45] (among many others). That analysis is not directly applicable here because he transformed his equations to an initial-value problem whose correspondence to the original formulation is rather intricate. The obvious limitations of the axisymmetry assumption inherent in these equations, coupled with the absence of bending rigidity, prevented him from pursuing in depth the possibility of wrinkling, but he proposed an approximate bifurcation criterion nonetheless. This stipulates that a *lower bound*, Λ_0^* (say), for the true wrinkling load corresponds to the value of $\Lambda > 0$ for which the membrane azimuthal stresses ($\mathring{N}_{\theta\theta}$ – see Appendix B) first vanish along the outer boundary. In the next section we are going to recover this result as a by-product of our perturbation scheme, without the need to postulate it as an external assumption. We remark in passing that by re-arranging some of Simmonds' equations [45] the authors of [27] found that the critical $\Lambda_{\rm v}$ in (2.5) must be $\mathcal{O}(\Omega^3)$, which is partly the motivation behind adopting the scaling (4.2). Our independent direct numerical simulations confirm this result as well.

A routine local analysis of the nonlinear differential equation (4.4) shows that close to the outer rim of the annulus equation (4.4) admits a regular solution

$$\Phi_0 \sim a_1(1-\rho) + \mathcal{O}\big((1-\rho)^2\big) + \dots\,, \qquad \text{as} \qquad \rho \to 1^-\,, \tag{4.6}$$

where $a_1 \in \mathbb{R}$ is an arbitrary constant that can be determined by specifying one additional condition at $\rho = 1$. In our scenario such extra constraint will come from the considerations mentioned in the preceding paragraph; this will be elaborated upon in §4.2, while further details about the local behaviour (4.6) are included in Appendix C. With the help of the first equation in (4.3) it is easily seen that Θ_0 is also regular near the outer rim.

The above observations suggest that locally, near $\rho = 1$, the functions Θ_0 and Φ_0 in (4.3) can be approximated by their corresponding Taylor series. Since the pre-buckling fields depend also on Λ, it is helpful to regard them as being functions of two variables, ρ and Λ; that is, $\Theta_0 \equiv \Theta_0(\rho;\Lambda)$ and

$\Phi_0 \equiv \Phi_0(\rho;\Lambda)$. The two-dimensional Taylor expansions of these functions around $(\rho,\Lambda) = (1,\Lambda_0)$, with $\Lambda_0 = \mathcal{O}(1)$ to be specified later, will involve the coefficients

$$\Pi_{pq} \equiv \Pi_{pq}(\Lambda_0) := \frac{\partial^{p+q}\Phi_0}{\partial\rho^p\partial\Lambda^q}(1;\Lambda_0)\,, \qquad \Gamma_{pq} \equiv \Gamma_{pq}(\Lambda_0) := \frac{\partial^{p+q}\Theta_0}{\partial\rho^p\partial\Lambda^q}(1;\Lambda_0) \tag{4.7}$$

for $p,q = 0,1,2,\ldots$; the calculation of these quantities will be postponed until we reach the next section.

Before proceeding to the simplification of the bifurcation equations, we emphasise that the basic-state terms that appear in the definitions of the coefficients $\mathcal{A}_{ijk}$ recorded in Appendix B will be replaced by $\Phi \to \Omega^2\Phi_0$ and $\Theta \to \Omega\Theta_0$. Essentially, the bending stiffness of the plate prior to the onset of buckling will be ignored. To gain a sense of the possible limitations or loss of accuracy that are introduced by this assumption, we have solved the bifurcation system (2.11) with the basic state given by (4.4)-(4.5). An illustrative set of comparisons between those results and the standard numerical calculations reviewed in §3 is included in Figure 7; there is hardly any difference between the transverse displacements W obtained via the two different routes. Further information is included in Figure 8, where we show similar comparisons for the pre-buckling azimuthal stresses at the onset of buckling. While the two sets of results in each window display some disagreement in the vicinity of $\rho = \eta$ (owing to the presence of a boundary layer [49] in the proximity of that location), this trend tends to diminish as Ω increases. More importantly, near the outer perimeter of the plate (where buckling is likely to develop) the effect of ignoring the bending stiffness of the base state appears to be inconsequential. We remark in passing that the features seen in the last two figures extend to a much broader set of values for η and ν than those considered here.

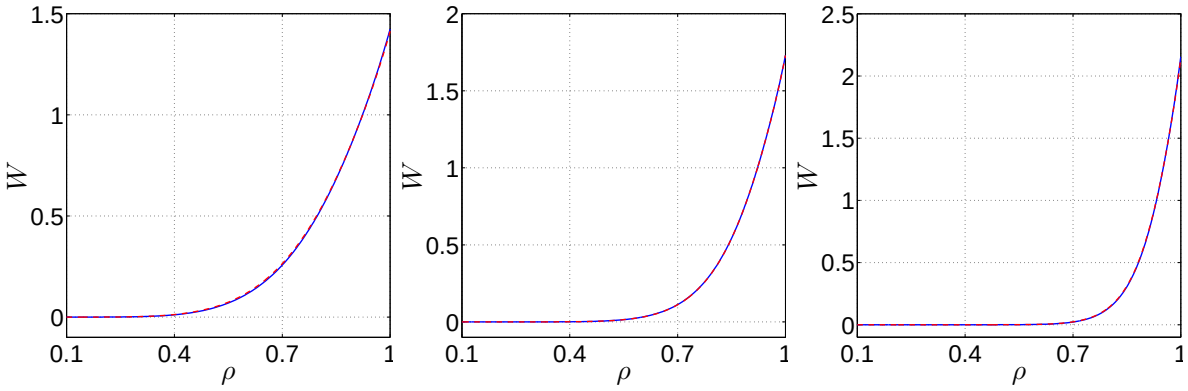

Figure 7: Comparisons between the *eigenmodal transverse displacements* of the bifurcation problem (2.11)–(2.13) in the case of a basic state corresponding to either the *plate* equations (2.5)-(2.7) or the *nonlinear membrane* simplification (4.4)-(4.5). The latter results are represented by dashed (red) lines, while the former are shown with continuous (blue) lines; from left to right, $\Omega = 50$, 100, and 200. In each window the two sets of curves are virtually indistinguishable. Here $\eta = 0.1$ and $\nu = 1/3$.

4.2 The bifurcation system

From the discussion in §3, we anticipate that in the limit $\Omega \gg 1$ the critical eigenmodes of the spinning disc are confined to a narrow zone attached to its outer rim. To identify the relevant scalings we start by writing $1-\rho = \Omega^{-q}Y$, with $q > 0$ to be found and $Y = \mathcal{O}(1)$. The key idea for the next step is

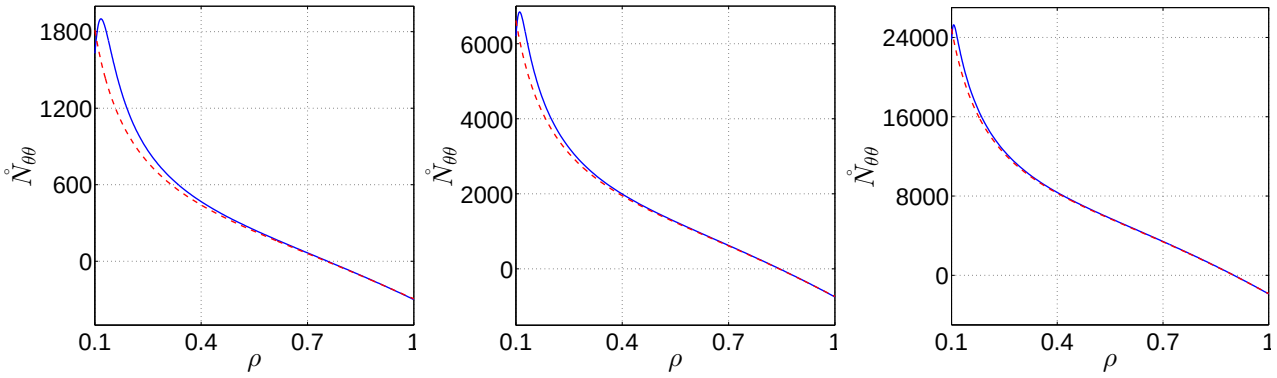

Figure 8: Illustration of the *azimuthal pre-buckling stresses* $\mathring{N}_{\theta\theta}$ associated with the scenarios included in Fig. 7. The same conventions apply here: the (red) dashed curves are used for the pure membrane situation (no bending stiffness), while the (blue) continuous curves pertain to the plate case (bending stiffness is accounted for in the pre-buckling range).

to attempt to choose our parameters (q, Λ, and m) such that the structure of the eigenmodes is set on the same radial length-scale as significant variation in the simplified basic state already discussed. Past experience indicates that the largest contribution in the equations (2.11) originate from the pre-buckling term in $\mathcal{A}_{110}W = \mathcal{O}(m^2\Omega^2)$, which in this case amounts to $\mathring{N}_{\theta\theta}(1)$ (see Appendix B). If a dash denotes differentiation with respect to Y, the second largest contribution would normally come from $\Phi \sim \Omega^2\Phi_0$ in the expression $\mathcal{A}_{112}W'' = \mathcal{O}(\Omega^{2+2q})$, but this is no longer true since in the present scenario $\Phi_0(1) = 0$. This leaves open the possibility that $W'''' = \mathcal{O}(\Omega^{4q})$ matches the size of the next-order terms in $\mathcal{A}_{110}$, which translates into $\Omega^{4q} \sim m^4 \sim m^2\Omega^{2-q}$, whereby $q = 2/3$ and $m = \mathcal{O}(\Omega^{2/3})$. We therefore conclude that the spatial structure of the critical eigenmodes includes an $\mathcal{O}(\Omega^{-2/3})$ boundary layer adjacent to $\rho = 1$. These preliminary observations set the stage for the next key development.

Motivated by the above discussion we introduce the streched coordinate $Y > 0$ defined by

$$\rho = 1 - \Omega^{-2/3}Y\,, \qquad Y = \mathcal{O}(1)\,, \tag{4.8}$$

and set $m^2 = \Omega^{4/3}M_0$ for some $M_0 = \mathcal{O}(1)$ (that will be recovered as part of the solution). We look for the quantities of interest with an ansatz of the form

$$\Lambda = \Lambda_0 + \Lambda_1\Omega^{-2/3} + \dots\,, \qquad (\Lambda_j \in \mathbb{R},\, j = 0, 1, \dots)\,, \tag{4.9a}$$

$$W = W_0(Y) + \Omega^{-2/3}W_1(Y) + \dots\,, \tag{4.9b}$$

$$F = \Omega^{-1/3}F_0(Y) + \Omega^{-1}F_1(Y) + \dots\,, \tag{4.9c}$$

where the constants Λ_j as well as the individual terms W_j, F_j on the right-hand side of (4.9) are found as usual by substituting the assumed solution in the differential equations (2.11), collecting like powers of Ω, and setting to zero the corresponding coefficients. We can begin to tackle this task by expanding the pre-buckling field Φ_0 as Taylor series taken about $(\rho, \Lambda) = (1, \Lambda_0)$, with Λ_0 the leading-order term in (4.9a). This shows that where $Y = \mathcal{O}(1)$ we have

$$\Phi_0 = \Omega^2\Pi_{00} + \Omega^{4/3}(\Lambda_1\Pi_{01} - \Pi_{10}Y) + \dots\,, \tag{4.10}$$

and by taking derivatives of (4.10) it follows that

$$\frac{d\Phi_0}{d\rho} = \Omega^{8/3}\Pi_{10} - \Omega^{4/3}(-\Lambda_1\Pi_{11} + \Pi_{20}Y) + \dots \,. \tag{4.11}$$

We remark that expressions analogous to (4.10) and (4.11) hold for Θ_0 and its derivative, with the Π_{pq} replaced by Γ_{pq} $(p, q = 0, 1, 2, \dots)$.

Returning to the main bifurcation system, it transpires that use of the ansatz (4.9) into (2.11) gives the zeroth-order equation

$$\Pi_{10} + 1 = 0 \quad \Longrightarrow \quad \frac{\partial\Phi_0}{\partial\rho}(1;\Lambda_0) = -1\,. \tag{4.12}$$

This now imposes a third condition on the second-order equation (4.4), and (4.12) can only be satisfied for a certain value $\Lambda = \Lambda_0^\dagger$ (say). It is this constraint that fixes the leading-order term in the expansion (4.9a). Comparing the first equation in (4.12) with the expression of $\mathring{N}_{\theta\theta}$ in (B.1) it should be clear that the former is equivalent to Simmonds' empirical wrinkling criterion [45] mentioned in §4.2, and thus $\Lambda_0^\dagger \equiv \Lambda_0^*$.

At next order we discover two (semi-)coupled differential equations, which are best discussed separately. The first one involves only the leading-order term W_0 in (4.9b) and assumes the form

$$\frac{d^4W_0}{dY^4} + \mathcal{B}_2(Y)\frac{d^2W_0}{dY^2} + \mathcal{B}_1\frac{dW_0}{dY} + \mathcal{B}_0(Y)W_0 = 0\,, \tag{4.13}$$

where

$$\mathcal{B}_2(Y) := -\big[(2M_0 + \Lambda_1\Pi_{01}^*) + Y\big]\,, \qquad \mathcal{B}_1 := \Pi_{10}^*\,, \tag{4.14a}$$

$$\mathcal{B}_0(Y) := M_0\big[(M_0 + \Lambda_1\Pi_{11}^*) - (\Pi_{20}^* + 2)Y\big]\,, \tag{4.14b}$$

and we have also introduced the notations

$$\Pi_{pq}^* := \Pi_{pq}(\Lambda_0^*) \qquad \text{and} \qquad \Gamma_{pq}^* := \Gamma_{pq}(\Lambda_0^*)\,.$$

Some immediate simplifications are available for the above coefficients; for example,

$$\Pi_{01}^* \equiv \frac{\partial\Phi_0}{\partial\Lambda}(1;\Lambda_0^*) = 0\,,$$

due to the second boundary condition in (2.7b). Furthermore, by letting $\rho \to 1$ and $\Lambda \to \Lambda_0^*$ in equation (4.4), we also find that

$$\Pi_{20}^* \equiv \frac{\partial^2\Phi_0}{\partial\rho^2}(1;\Lambda_0^*) = -\frac{1}{2}\Lambda_0^{*2} - (\nu + 2)\,. \tag{4.15}$$

Comparing (4.15) with the expressions given in Appendix C, it is clear that Π_{20}^* is the same as $2a_2$ in which $a_1 \to 1$ and $\Lambda \to \Lambda_0^*$.

With this information in hand, equation (4.13) can then be cast as

$$\frac{d^4W_0}{dY^4} - \frac{d}{dY}\left[(2M_0 + Y)\frac{dW_0}{dY}\right] + M_0\left[\big(M_0 + \Lambda_1\Pi_{11}^*\big) + \left(\nu + \frac{1}{2}\Lambda_0^{*2}\right)Y\right]W_0 = 0\,, \tag{4.16}$$

and it is recalled that (4.16) must be solved subject to the boundary constraints that follow from (2.13b) and (2.13c), i.e.

$$\frac{d^2W_0}{dY^2} - \nu M_0 W_0 = 0\,, \qquad \text{for} \quad Y = 0\,, \tag{4.17a}$$

$$\frac{d^3W_0}{dY^3} - (2-\nu)M_0\frac{dW_0}{dY} = 0\,, \qquad \text{for} \quad Y = 0\,, \tag{4.17b}$$

as well as the decay conditions

$$W_0\,, \quad \frac{dW_0}{dY} \to 0 \qquad \text{as} \quad Y \to +\infty\,. \tag{4.18}$$

Note that (4.16) together with the constraints (4.17) and (4.18) constitute an eigenvalue problem in which the eigenparameter Λ_1 depends on $M_0 > 0$. Since we are ultimately interested in the critical buckling load, the aim is to minimise (numerically) the function $\Lambda_1 = \Lambda_1(M_0)$ (e.g., see [46, 47, 48]). A standard numerical solution allows us to identify the value $M_0 = M_0^*$ for which the eigenvalue Λ_1 is least, Λ_1^* (say). Before we can put this into practice we still need to compute Π_{11}^*, and this is explained next. To this end, let us introduce the new function

$$\Psi_0(\rho;\Lambda) := \frac{\partial\Phi_0}{\partial\Lambda}(\rho;\Lambda)\,, \qquad \eta \le \rho \le 1\,. \tag{4.19}$$

Differentiation of (4.4) with respect to Λ, followed by the substitution $\Lambda \to \Lambda_0^*$, yields

$$\mathcal{L}_0[\Psi_0] + \frac{\Lambda_0^*}{4\Phi_0^3}\left[\frac{(1-\rho^2)^2}{\rho}\right](\Phi_0 - \Lambda_0^*\Psi_0) = 0\,. \tag{4.20}$$

The corresponding boundary conditions for this second-order differential equations are obtained by a similar differentiation process in (4.5), thus leading to

$$\frac{\partial\Psi_0}{\partial\rho}(\eta;\Lambda_0^*) - \left(\frac{\nu}{\eta}\right)\Psi_0(\eta;\Lambda_0^*) = 0\,, \qquad \Psi_0(1;\Lambda_0^*) = 0\,. \tag{4.21}$$

Equations (4.4) and (4.20) are solved simultaneously subject to (4.5) and (4.21). Once this is completed, we recover the quantity of interest via

$$\Pi_{11}^* \equiv \frac{\partial\Psi_0}{\partial\rho}(1;\Lambda_0^*)\,.$$

For completeness, we summarise below the final asymptotic results

$$\Lambda_{\rm v}^{(c)} \simeq \Lambda_0^*(\eta,\nu)\Omega^3 + \Lambda_1^*(\eta,\nu)\Omega^{7/3} + \dots\,, \qquad m_c \simeq \sqrt{M_0^*(\eta,\nu)}\,\Omega^{2/3} + \dots\,. \tag{4.22}$$

As hinted by our notations in these formulae, it is clear that the numerical calculations required to obtain the final form of (4.22) will depend on both the in-plane aspect ratio of the annular plate (η) and the Poisson's ratio (ν). If we take $\nu = 1/3$ and $\eta = 0.1$, we find $\Lambda_0^* \simeq 0.550641$, $\Lambda_1^* \simeq 4.458345$, and $M_0^* \simeq 0.441538$ ($\Pi_{11}^* \simeq -0.366267$). The accuracy of the above two asymptotic formulae for these particular values is illustrated in Figure 9. The relative errors for the critical $\Lambda_{\rm v}^{(c)}$ are below 0.22%, while those for the mode number are about 2.5% (or smaller). In both cases, the formulae (4.22) provide a tight *upper bound* for the "true" values obtained by direct numerical integration of

the original bifurcation problem. This upper-bound feature is a direct consequence of neglecting the bending stiffness in the pre-buckling range. Unlike in some of our recent studies (e.g., [57, 58]), in which we encountered oscillatory asymptotic approximations for the eigenvalues of similar fourth-order bifurcation problems, here the situation is different and it is very unlikely that the computation of any number of additional terms in (4.9a) will change the nature of the approximation. We note also that the leading-order problem (4.16) cannot be solved in terms of special functions, so the calculation of Λ_2 in (4.9a) is a purely numerical affair. Given the excellent accuracy for the critical transverse load, it is questionable whether the effort required to evaluate that term (or the next few ones) would be commensurate with any potential benefits; note that the calculation of further terms in the asymptotic ansatz (4.9) would also require a revision of the Taylor series (4.10) and (4.11). The good agreement seen in Figure 9 is representative for other values of η and ν, but in the interest of brevity we do not pursue this quantitative aspect further.

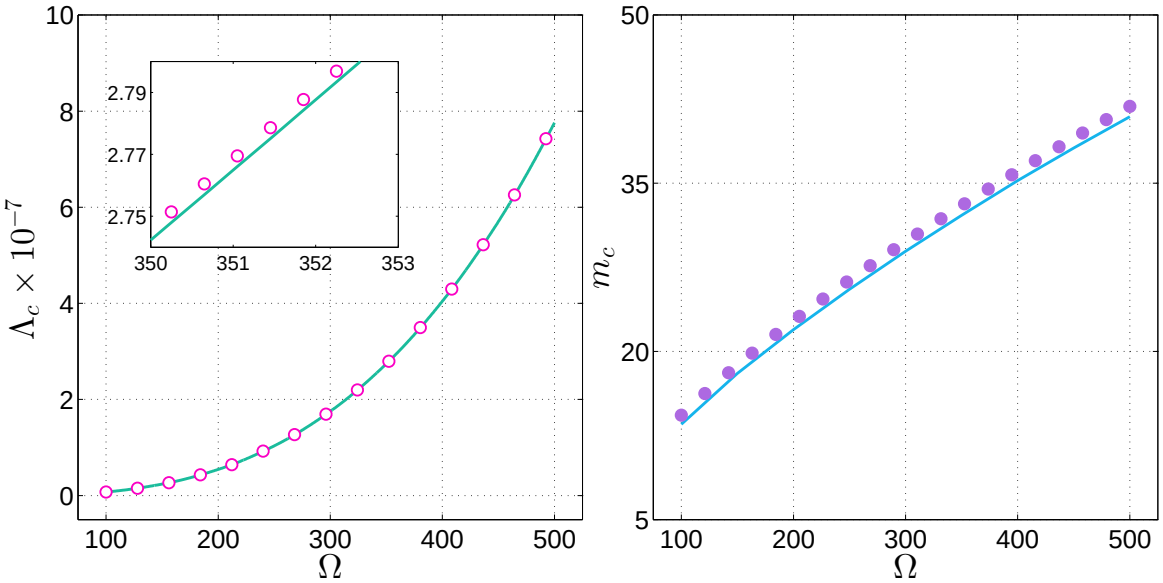

Figure 9: Comparisons between the asymptotic predictions (4.22) and direct numerical simulations of the wrinkling equations (2.11) subject to the boundary conditions (2.12) and (2.13). In each window, the latter data are shown with the continuous line, while the round markers represent the asymptotic approximations. The inset in the left window clarifies the relative positions of these two sets of data. Here $\eta = 0.1$ and $\nu = 1/3$.

Before concluding our discussion regarding the proposed asymptotic simplification of the wrinkling system (2.11), a number of brief remarks about its second equation are in order. Use of the ansatz (4.9) in that equation yields

$$\mathcal{L}_{\#}[F_0] = M_0^* \Gamma_{10}^* W_0 - \Gamma_{00}^* \frac{d^2 W_0}{dY^2}\,, \tag{4.23}$$

where we have introduced the homogeneous differential operator

$$\mathcal{L}_{\#} := \frac{d^4}{dY^4} - 2M_0^* \frac{d^2}{dY^2} + M_0^{*2} \equiv \left(\frac{d^2}{dY^2} - M_0^*\right)^2 .$$

Equation (4.23) must be solved subject to the boundary conditions

$$F_0 = \frac{dF_0}{dY} = 0\,, \qquad \text{for} \quad Y = 0\,, \tag{4.24}$$

as well as the decay conditions

$$F_0\,, \quad \frac{dF_0}{dY} \to 0 \qquad \text{as} \quad Y \to +\infty\,. \tag{4.25}$$

In light of the work carried out in the first part of this section it transpires that the reduced problem for F_0 plays only a secondary role since there is no new information regarding (4.9a) that emerges from its solution. To complete the determination of F_0 we need the Γ-coefficients on the right-hand side of (4.23). Routine algebraic manipulations of (4.3) and (4.15) indicate that these are readily available in terms of quantities already computed, namely

$$\Gamma^*_{00} = \Lambda^*_0 \qquad \text{and} \qquad \Gamma^*_{10} = -\frac{1}{4}\Lambda^*_0\big[2(1+\nu) + \Lambda^{*2}_0\big]\,. \tag{4.26}$$

The presence of W_0 and its second-order derivative on the right-hand side of (4.23) suggests that this equation is best solved simultaneously together with (4.16). A comparison between the leading-order functions in (4.9) and the corresponding results of direct numerical simulations of (2.11) subject to (2.12)-(2.13) is illustrated in Figure 10. In the interest of brevity, only one case is shown ($\eta = 0.1$, $\nu = 1/3$, and $\Omega = 400$), but the agreement seen there is characteristic for all the other cases we have tested. It is clear that for sufficiently large Ω the asymptotic predictions match very closely the direct numerical simulations, hence providing further evidence in support of the solution strategy proposed above.

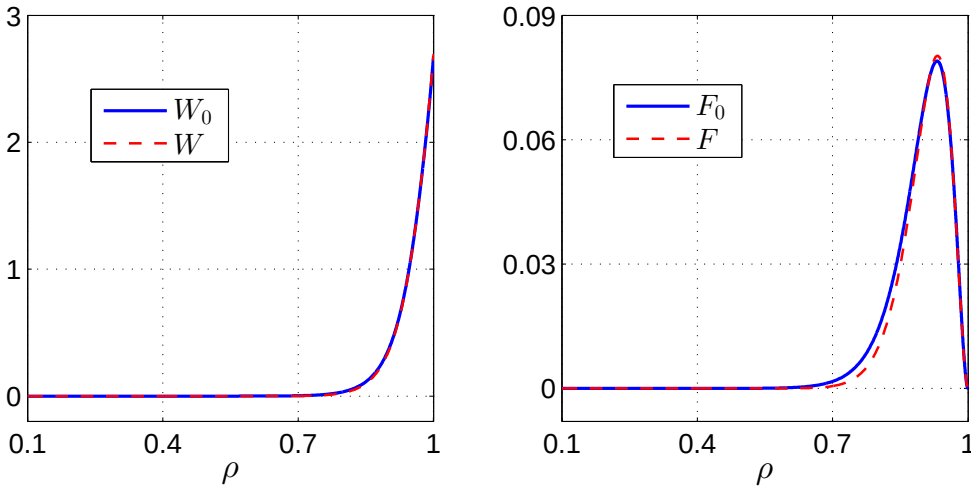

Figure 10: Comparisons of the leading-order terms in the asymptotic expansions (4.9b)-(4.9c) with the corresponding direct numerical simulations of the original bifurcation system discussed in §2. In this example, $\eta = 0.1$, $\nu = 1/3$, and $\Omega = 400$.

5 Discussion

We have considered a possible asymptotic approximation of a wrinkling problem [27] recently proposed in connection with a normally loaded, spinning, thin annular plate. One of the motivations behind

our study has been to elucidate the possible connections with some related earlier work on similar (tensile) wrinkling instabilities (e.g., [32, 33, 36]), and in which it was shown that the the linearised FvK bifurcation system can be asymptotically decoupled. While this feature still persists in the currently proposed simplification strategy as well, the situation is in fact rather different. In the works just mentioned, the behaviour of the plate was dominated by stretching, so the entire asymptotic structure of the bifurcation system turned out to be controlled by a hierarchy of *second-order* Airy-like equations in the transverse displacement. In addition, the corresponding stress function was only algebraically related to the transverse displacement and its derivatives. For the approximation scheme considered in this paper it transpired that the bending and stretching effects are actually comparable in the simplified model, which was the main reason why we ended up with the *fourth-order* reduced equation (4.13). Also, the decoupling of the two equations in the FvK system is now only partial, in the sense that one is still left with solving an inhomogeneous fourth-order differential equation with constant coefficients in order to recover the stress function. Similar situations were previously encountered in the context of pure bending of cylindrical shells [46, 47, 54], twisting of stretched thin elastic strips [48], and pressurised thin shallow spherical caps [59].

Although we have succeeded in obtaining a (simplified) asymptotic characterisation of both the critical load and the corresponding mode number – see (4.22), one inconvenient complication in these formulae is the implicit dependence on the non-dimensional parameters $0 < \eta < 1$ and $0 < \nu \leq 0.5$. In principle, one can compute the coefficients that appear in (4.22) for a discrete set of values of these two parameters, and then rely on suitable interpolation techniques to find an estimate for any other values of interest. This is a purely quantitative task that falls outside the main scope of this study; similar limitations were encountered in reference [47, 59], to which we refer for more details.

Notwithstanding the apparent dynamic nature of the phenomena explored in this paper, the main bifurcation problem is a conservative one, a fact that was apparently overlooked in the previous investigations (e.g., [27]). This property is related to the fact that centrifugal forces are conservative if the angular speed is constant in time. When coupled with the FvK plate theory, which admits a variational formulation, it is unsurprising that the outcome is essentially a conservative stability problem. The explicit arguments for establishing the self-adjointness of the wrinkling problem summarised in §2 are tedious, but entirely elementary; we refer to the related work of Adams [37] which contains an outline of the key steps for a similar set of equations. It is well known and widely documented (e.g., see [61, 62]) that the dynamic and static approaches to buckling problems in elasticity are equivalent to each other if the problems in question are conservative. It is for this reason that we have pursued the latter route in our numerical investigations.

In keeping with the earlier study of Delapierre *et al.* [27], in this work linear isotropy was assumed for the material of the annular disc. This constitutive assumption can be relaxed and one can consider instead polar orthotropy, as was done in [60] for a different wrinkling scenario. We expect the qualitative features of our analysis as applied to the new configuration to remain the same as long as the outer edge of the spinning disc is still taken to be stress-free. As explained in connection with the scaling analysis at the beginning of §4.2, the asymptotic balancing of the various terms in the first equation of the system (2.11) requires a contribution from the bending term because of the condition $\Phi(1) = 0$. It would be of interest to investigate a modification of the current spinning disc set-up by considering a heavy ring attached to the outer edge of (and rotating with) the disc. In that case the outer rim is no longer stress-free, so the extent to which the conclusions of the work reported herein hold true is not immediately obvious.

One of the key ingredients in our analysis was the assumption that a reasonably accurate approximation of the pre-buckling state is captured by the nonlinear membrane equation (4.4). Although this hypothesis was backed up by the various numerical examples included in this paper, there are

a few more subtle features that deserve some comments. Lin and Wan [63] proposed a comprehensive mathematical classification of the interplay between bending and stretching effects in the *radially symmetric* deformations experienced by a normally loaded spinning membrane. By introducing the non-dimensional parameters

$$0 < \varepsilon := (\nu+3)^{-1}\Omega^{-2} \ll 1\,, \qquad \mu_\ell := \varepsilon\Lambda_{\rm v}^{2/3}\,, \tag{5.1}$$

they suggested that the case $0 < \mu_\ell < 1$ corresponds to the so-called *'relatively fast spinning'* (RFS) disc; on the other hand, for $\mu_\ell > 1$ the plate would be expected to experience significant bending throughout, a situation that Lin and Wan labelled the *'relatively high pressure'* (RHP) range. The difference between these regimes is quite pronounced, at least mathematically. For RFS the nonlinear system (2.5)-(2.7) can be reduced to a sequence of linear problems, with the bending and stretching effects being only weakly coupled, whereas for RHP the Hencky-Föppl equation plays the role of an outer asymptotic expansion that has to be augmented by suitable boundary layers near the inner and outer rims of the disc. According to Lin and Wan's above categorisation, the scenario discussed in this paper would fall under the first regime (i.e., RFS). Numerical evidence in support of this statement is included in Figure 11, which shows the dependence of $\mu_\ell = \mu_\ell(\Omega)$ for $100 \le \Omega \le 500$ in two cases ($\eta = 0.1$ and $\eta = 0.5$). The reason for this apparent discrepancy between our work and that of [63] is twofold. First, unlike in the latter reference, the critical transverse load in the present context is dependent on Ω via the eigenproblem discussed in §2, so ε and μ_ℓ defined in (5.1) cannot be varied independently of each other; in this regard, the criterion $0 < \mu_\ell < 1$ proposed by Lin and Wan is misleading unless further restrictions are spelled out. The second reason mentioned above is best understood by outlining the decoupling of the system (2.5) as proposed by those authors.

To this end, we re-scale the pre-buckling fields Θ and Φ by setting (cf. [63])

$$\Theta(\rho) =: \varepsilon\Lambda_{\rm v}\widehat{\Theta}(\rho) \qquad \text{and} \qquad \Phi(\rho) =: \varepsilon^{-1}\widehat{\Phi}(\rho)\,, \tag{5.2}$$

so that (2.5) becomes

$$\varepsilon\mathcal{L}_0[\widehat{\Theta}] - \frac{\widehat{\Theta}\widehat{\Phi}}{\rho} = \left(\frac{\rho^2-1}{2\rho}\right), \qquad \mathcal{L}_0[\widehat{\Phi}] + \mu_\ell^3\left(\frac{\widehat{\Theta}^2}{2\rho}\right) = -\rho\,. \tag{5.3}$$

In reference [63] it was suggested that the solution of the above re-scaled system can be sought with an ansatz of the form

$$\{\widehat{\Theta},\widehat{\Phi}\} = \sum_{k=0}^{\infty}\{\widehat{\Theta}_k,\widehat{\Phi}_k\}\mu_\ell^{3k}\,, \tag{5.4}$$

where $\widehat{\Theta}_k \equiv \widehat{\Theta}_k(\rho)$ and $\widehat{\Phi}_k \equiv \widehat{\Phi}_k(\rho)$ ($k = 0, 1, 2, \dots$) are functions to be found. While this has the merit of decoupling the two equations in (2.5), the $\widehat{\Theta}_k$ terms will satisfy a sequence of singularly-perturbed second-order differential equations. The individual asymptotic expansions of these terms will each be a sum of further terms, which in turn leads to (5.4) being a multiple sum that is not easily ordered (in an asymptotic sense) unless one introduces additional assumptions about the relative sizes of ε and μ_ℓ (or powers of them); this is, however, a moot point in [63]. Another way of looking at (5.3) would be to consider ε rather than μ_ℓ^3 as the "working" asymptotic parameter. In that case, the nonlinear membrane equation (4.4) corresponds to an outer asymptotic approximation for the aforementioned system. This conclusion is trivially reached by setting $\widehat{\Theta} \to \widehat{\Theta}_{\rm out} \equiv \widehat{\Theta}_0(\rho) + \dots$ and $\widehat{\Phi} \to \widehat{\Phi}_{\rm out} \equiv (\nu+3)^{-1}\widehat{\Phi}_0(\rho) + \dots$, and then making use of the definitions (5.1); the outcome of these manipulations is that $\widehat{\Phi}_0$ satisfies (4.4) in §4.1. The outer solution can be augmented by two boundary

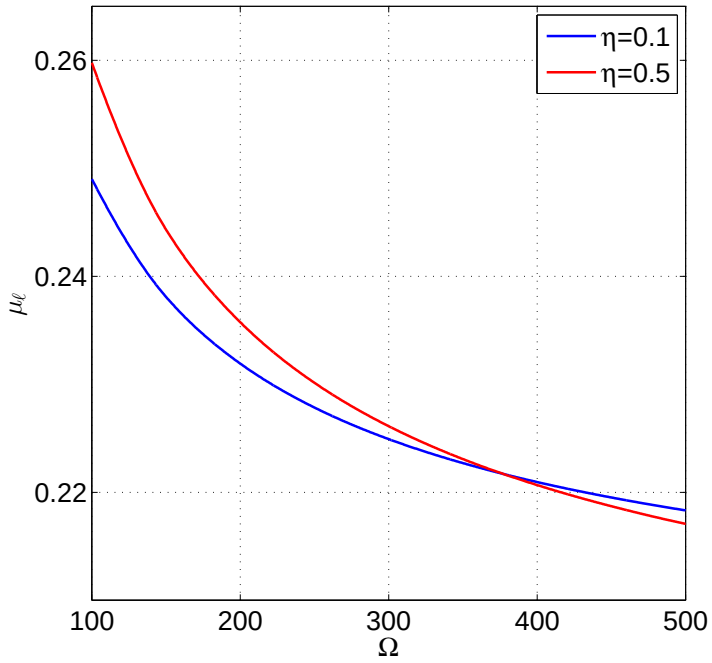

Figure 11: The dependence of Lin and Wan's ([63]) parameter μ_ℓ defined in (5.1) on the non-dimensional angular speed $\Omega \gg 1$; here $\nu = 1/3$.

layers of thicknesses $\mathcal{O}(\varepsilon^{1/2})$ and $\mathcal{O}(\varepsilon^{1/3})$ attached to the locations $\rho = \eta$ and $\rho = 1$, respectively. It is interesting to note that the latter boundary layer involves only $\widehat{\Theta}$, an observation that explains the excellent accuracy of the asymptotic formulae obtained (recall that the reduced equation (4.13) contains only terms from the differential operator $\mathcal{L}_{11}$, whose coefficients do not depend on Θ). On the other hand, the slight discrepancy in the approximation of F seen in the right window of Figure 10 can be traced back to ignoring the $\mathcal{O}(\Omega^{-2/3})$ layer in the pre-buckling field Θ. We were fortunate that the determination of the first two terms in the approximation of the critical load – see (4.22), did not hinge on using those ignored terms. A more detailed discussion of these and related issues will be reported in a forthcoming study [49].

A General boundary conditions for (2.4)

For the sake of completeness we record here the dimensional version of the boundary conditions that can be specialised to yield equations (2.7), (2.12), and (2.13).

The clamped edge of the plate ($r = R_1$) requires the following constraints

$$w = \frac{\partial w}{\partial r} = 0\,, \tag{A.1a}$$

$$\frac{\partial^2 f}{\partial r^2} - \frac{\nu}{r}\left[\frac{\partial f}{\partial r} + \frac{1}{r}\left(\frac{\partial^2 f}{\partial \theta^2}\right)\right] - \frac{1}{2}(1-\nu)\rho_m h\omega^2 r^2 = 0\,, \tag{A.1b}$$

$$\frac{\partial}{\partial r}\left[\frac{\partial^2 f}{\partial r^2}+\frac{1}{r}\left(\frac{\partial f}{\partial r}\right)\right]+\frac{1}{r^2}\frac{\partial^2}{\partial\theta^2}\left[(2+\nu)\frac{\partial f}{\partial r}-(3+\nu)\frac{f}{r}\right]-(1-\nu)\rho_m h\omega^2 r=0\,, \tag{A.1c}$$

while along the free edge ($r=R_2$) the following conditions apply

$$\frac{\partial}{\partial r}\left(\nabla^2 w\right)+\frac{1}{r^2}(1-\nu)\frac{\partial^2}{\partial\theta^2}\left(\frac{\partial w}{\partial r}-\frac{w}{r}\right)=0\,, \tag{A.2a}$$

$$\frac{\partial^2 w}{\partial r^2}+\frac{\nu}{r}\left[\frac{\partial w}{\partial r}+\frac{1}{r}\left(\frac{\partial^2 w}{\partial\theta^2}\right)\right]=0\,, \tag{A.2b}$$

$$\frac{\partial f}{\partial r}+\frac{1}{r}\left(\frac{\partial^2 f}{\partial\theta^2}\right)-\frac{1}{2}\omega^2 r^3=0\,, \tag{A.2c}$$

$$-\frac{\partial^2 f}{\partial r\partial\theta}+\frac{1}{r}\left(\frac{\partial f}{\partial\theta}\right)=0\,. \tag{A.2d}$$

B Coefficients of the bifurcation equations

The coefficients $\mathcal{A}_{ijk}$ that appear in the definitions of the operators $\mathcal{L}_{ij}$ for the eigensystem (2.11) are listed below. In particular, in $\mathcal{L}_{11}$ and $\mathcal{L}_{22}$ we have

$$\mathcal{A}_{114}=1\,, \qquad \mathcal{A}_{224}=\mathcal{A}_{114}\,,$$

$$\mathcal{A}_{113}=\frac{2}{\rho}\,, \qquad \mathcal{A}_{223}=\mathcal{A}_{113}\,,$$

$$\mathcal{A}_{112}=-\left[\left(\frac{2m^2+1}{\rho^2}\right)+\frac{\Phi}{\rho}\right], \qquad \mathcal{A}_{222}=-\left(\frac{2m^2+1}{\rho^2}\right),$$

$$\mathcal{A}_{111}=\frac{1}{\rho}\left[\left(\frac{2m^2+1}{\rho^2}\right)-\frac{d\Phi}{d\rho}\right], \qquad \mathcal{A}_{221}=\frac{1}{\rho}\left(\frac{2m^2+1}{\rho^2}\right),$$

$$\mathcal{A}_{110}=\frac{m^2}{\rho^2}\left[\left(\frac{m^2-4}{\rho^2}\right)+\underline{\frac{d\Phi}{d\rho}+\Omega^2\rho^2}\right], \qquad \mathcal{A}_{220}=\frac{m^2}{\rho^2}\left(\frac{m^2-4}{\rho^2}\right).$$

The coefficients in $\mathcal{L}_{12}$ and $\mathcal{L}_{21}$ are

$$\mathcal{A}_{122}=-\frac{\Theta}{\rho}\,, \qquad \mathcal{A}_{212}=-\mathcal{A}_{122}\,,$$

$$\mathcal{A}_{121}=-\frac{1}{\rho}\left(\frac{d\Theta}{d\rho}\right), \qquad \mathcal{A}_{211}=-\mathcal{A}_{121}\,,$$

$$\mathcal{A}_{120}=\frac{m^2}{\rho^2}\left(\frac{d\Theta}{d\rho}\right), \qquad \mathcal{A}_{210}=-\mathcal{A}_{120}\,.$$

We mention also that the re-scaled *prebuckling membrane stresses* are given by

$$\mathring{N}_{rr}\equiv\frac{\Phi}{\rho} \qquad \text{and} \qquad \mathring{N}_{\theta\theta}\equiv\frac{d\Phi}{d\rho}+\Omega^2\rho^2\,, \tag{B.1}$$

with the latter expression corresponding to the underlined terms in $\mathcal{A}_{110}$.

C Local behaviour of the membrane basic state

The local behaviour of the solutions for the membrane basic state close to the outer rim was discussed briefly in §4.1. We record here a few coefficients in the asymptotic behaviour of $\Phi_0(\rho)$. For $\rho \to 1^-$,

$$\Phi_0(\rho) \sim \sum_{k=1}^{4} a_k (1-\rho)^k + \mathcal{O}\left((1-\rho)^5\right) , \tag{C.1}$$

where

$$a_2 := \frac{1}{2}a_1 - \frac{1}{2}(3+\nu) - \frac{\Lambda^2}{4a_1^2} , \qquad a_3 := \frac{1}{2}a_1 - \frac{(\nu+3)\Lambda^2}{12a_1^3} - \frac{\Lambda^4}{24a_1^5} ,$$

$$a_4 := \frac{1}{2}a_1 - \frac{1}{8}(\nu+3) - \frac{\Lambda^2}{16a_1^2}\left(\frac{13\Lambda^4}{72a_1^6} - \frac{\Lambda^2}{3a_1^3} + 1\right) - \frac{\Lambda^2(\nu+3)}{8a_1^3}\left(\frac{11\Lambda^2}{36a_1^3} + \frac{\nu+3}{4a_1} - \frac{1}{3}\right) ,$$

and $a_1 \in \mathbb{R}$ is arbitrary; in the present context it can be identified as explained in §4.2 – see equation (4.12).

Although, strictly speaking, this result is expected to be valid only in a very small vicinity of $\rho = 1$, it is interesting to note that the series (C.1) mimics quite closely the behaviour of the pre-buckling stress function Φ obtained from the *plate equations* (2.5)-(2.7). A couple of illustrative comparisons are included in Figure 12; relatively close to the outer rim the agreement between the two curves is better than 80%.

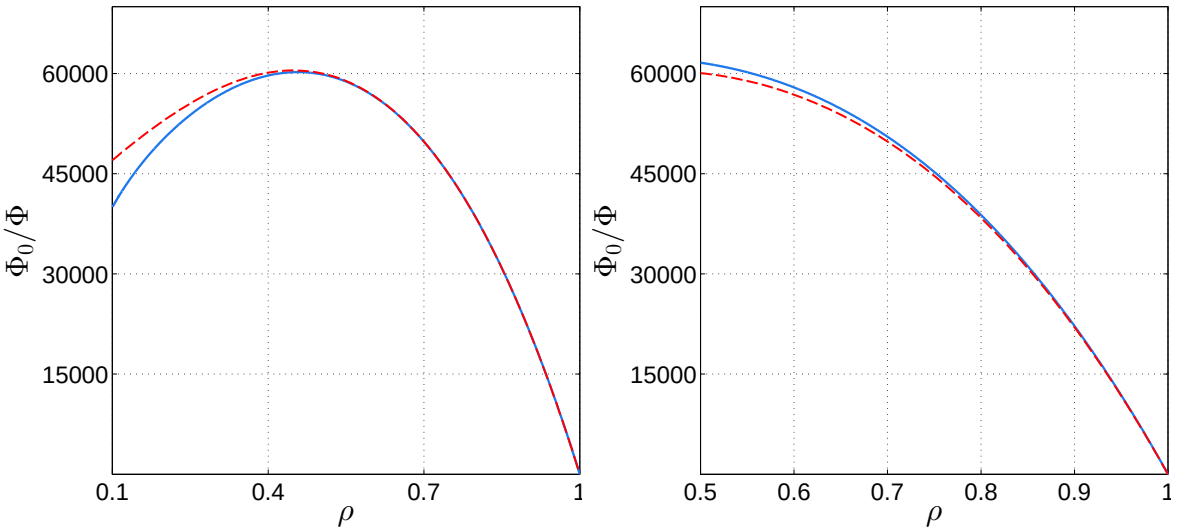

Figure 12: Comparison between the local approximation $\Omega^2\Phi_0(\rho)$ given by (C.1) with $a_1 \to 1$, $\Lambda \to \Lambda_0^*$, and the radially symmetric stress function $\Phi(\rho)$ obtained from the numerical solution of (2.5)-(2.7) for $\Lambda \to \Lambda_0^*\Omega^3$. The latter result is shown as a (blue) continuous curve, while the former corresponds to the (red) dashed curve. Here $\Omega = 500$, $\nu = 1/3$; $\eta = 0.1$ (left) and $\eta = 0.5$ (right),

References

[1] Love, A.: Mathematical Theory of Elasticity (Third Edition). Cambridge University Press, Cambridge (1920)

[2] Timoshenko, S.: Theory of Elasticity. McGraw-Hill Book Company, New York (1934)

[3] Prescott, J.: Applied Elasticity. Dover Publications, New York (1946)

[4] Sechler, E.E.: Elasticity in Engineering. Dover Publications, New York (1968)

[5] Singh, S.: Theory of Elasticity. Khanna Publishers, New Delhi (2018)

[6] Stodola, A.: Gas Turbines. D. van Nostrand Company, New York (1905)

[7] Tumarkin, S.: Methods of stress calculation in rotating disks. NACA Technical Memorandum (No. 1064), Washinton D.C. (1944)

[8] Rao, J.S.: History of Rotating Machinery Dynamics. Springer, Dordrecht (2011)

[9] Lamb, H., Southwell, R.V.: The vibration of a spinning disk. Proceedings of the Royal Society of London A **99**, 272–280 (1921)

[10] Southwell, R.V.: On the free vibrations of a uniform circular disc clamped at its centre; and on the effects of rotation. Proceedings of the Royal Society of London A **99**, 133–153 (1922)

[11] Simmonds, J.G.: The transverse vibrations of a flat spinning membrane. Journal of the Aeronautical Sciences **29**, 16–18 (1962)

[12] Eversman, W., Dodson, R.O.: Free vibration of a centrally clamped spinning circular disk. AIAA Journal **7**, 2010–2012 (1969)

[13] Pearson, R.T.: The development of the flexible-disk magnetic recorder. Proceedings of the IRE **49**, 164–174 (1961)

[14] Pelech, I., Shapiro, A.H.: Flexible disk rotating on a gas film next to a wall. ASME Journal of Applied Mechanics **31**, 577–584 (1964)

[15] Benson, R.C., Bogy, D.B.: Deflection of a very flexible spinning disk due to a stationary transverse load. ASME Journal of Applied Mechanics **45**, 636–642 (1978)

[16] Benson, R.C.: Observations on the steady-state solution of an extremely flexible spinning disk with a transverse load. ASME Journal of Applied Mechanics **50**, 525–530 (1983)

[17] Adams, G.G.: Analysis of the flexible disk/head interface. Journal of Tribology **102**, 86–90 (1980)

[18] Adams, G.G.: Critical speeds for a flexible spinning disk. International Journal of Mechanical Sciences **29**, 525–531 (1987)

[19] Ono, K., Chen, J-S., Bogy, D.B.: Stability analysis for the head/disk interface in a flexible disk drive. ASME Journal of Applied Mechanics **58**, 1005–1014 (1991)

[20] Carpino, M.: The effect of initial curvature in a flexible disk rotating near a flat plate. Journal of Tribology **113**, 355–360 (1991)

[21] Hosaka, H., Crandall, S.H.: Self-excited vibrations of a flexible disk rotating on an air film above a flat surface. Acta Mechanica (Supplement,vol.3) **3**, 115–127 (1992)

[22] D'Angello, C., Mote, C.D.: Aerodynamically excited vibration and flutter of a thin disk rotating at supercritical speed. Journal of Sound Vibration **168**, 15–30 (1993)

[23] Huang, F.Y., Mote, C.D.: On the instability mechanisms of a disk rotating close to a rigid surface. ASME Journal of Applied Mechanics **62**, 765–771 (1995)

[24] Nowinski, J.L: Nonlinear transverse vibrations of a spinning disk. ASME Journal of Applied Mechanics **31**, 72–78 (1964)

[25] Baddour, N., Zu, J.W.: A revisit of spinning disk models. Part I: derivation of equations of motion. Applied Mathematics Modelling **25**, 541–559 (2000)

[26] Chen, J-S.: On the linearization of the equations of motion of a rotating disk. Applied Mathematics Modelling **35**, 392–397 (2011)

[27] Delapierre, M., Chakraborty, D., Sader, J.E., Pellegrino, S.: Wrinkling of transversely loaded spinning membranes. International Journal of Solids and Structures **139-140**, 163–173 (2018)

[28] Lord Rayleigh: The problem of the whispering gallery. Philosophical Magazine **20**, 1001–1004 (1910)

[29] Lord Rayleigh: Further applications of Bessel's functions of high order to the whispering gallery and allied problems. Philosophical Magazine **27**, 100–109 (1914)

[30] Wright, O.: Gallery of whispers. Physics World **25**, 31–36 (2012)

[31] Coman, C.D.: Axisymmetric bifurcations in a pressurised circular thin plate under initial tension. Mechanics Research Communications **47**, 11-17 (2013)

[32] Coman, C.D., Matthews, M.T., Bassom, A.P.: Asymptotic phenomena in pressurised thin films. Proceedings of the Royal Society of London A **471**, 20150471 (2015)

[33] Coman, C.D., Bassom, A.P.: Singularities and wrinkling: the case of a concentrated force. International Journal of Engineering Science **126**, 229–244 (2016)

[34] Coman, C.D., A.P. Bassom: On the nonlinear membrane approximation and edge-wrinkling.. International Journal of Solids and Structures **82**, 85–94 (2008)

[35] Coman, C.D., Bassom, A.P.: On the role of in-plane compliance in edge wrinkling. Journal of Elasticity **126**, 135–154 (2017)

[36] Coman, C.D., Bassom, A.P.: Wrinkling structures at the rim of an initially stretched circular thin plate subjected to transverse pressure. SIAM Journal of Applied Mathematics **78**, 1009–1029 (2018)

[37] Adams, G.G.: Elastic wrinkling of a tensioned circular plate using von Kármán plate theory. ASME Journal of Applied Mechanics **60**, 520–525 (1993)

[38] Nayfeh, A.H.: Nonlinear Interactions. Wiley & Sons, New York (2000)

[39] Brush, Don O., Almroth, Bo O.: Buckling of Bars, Plates and Shells. McGraw-Hill Book Company, New York (1975)

[40] Niordson, F.I..: Shell Theory. North-Holland, Amsterdam (1985)

[41] Ventsel, E., Krauthammer, T.: Thin Plates and Shells: Theory, Analysis, and Applications. Marcel Dekker, Inc., New York (2001)

[42] Coman, C.D.: Continuum Mechanics and Linear Elasticity. Springer, Dordrecht (2020)

[43] Coman, C.D: Remarks on elastic buckling for sectorial plates. International Journal of Engineering Science **47**, 1002–1013 (2009)

[44] Weinitschke, H.J.: Some mathematical problems in the non-linear theory of elastic membranes, plates and shells. In : *Trends in Applications of Pure Mathematics to Mechanics*, G. Fichera (Ed.), 409–424. Pitman Publishing: London (1976)

[45] Simmonds, J.G: The finite deflection of a normally loaded, spinning elastic membrane. Journal of Aerospace Science **29**, 1180–1189 (1962)

[46] Coman, C.D.: Asymptotic approximations for pure bending of thin cylindrical shells. Zeitschrift für Angewandte Mathematik und Physik **68:82** (2017)

[47] Coman, C.D.: Oval cylindrical shells under asymmetric bending: a singular-perturbation solution. Zeitschrift für Angewandte Mathematik und Physik **69:120** (2018)

[48] Coman, C.D., A.P. Bassom: An asymptotic description of the elastic instability of twisted thin elastic plates. Acta Mechanica **200**, 59–68 (2008)

[49] Coman, C.D: On the asymptotic structure of edge-wrinkling in a normally loaded spinning disc. (in preparation)

[50] Sheploak, M., Dugundji, J.: Large deflections of clamped circular plates under initial tension and transitions to membrane behaviour. Journal of Applied Mechanics **65**, 107–115 (1998)

[51] Komaragiri, U.,Begley, M.R., Simmonds, J.G.: The mechanical response of free standing circular elastic films under point and pressure loads. Journal of Applied Mechanics **72**, 203–212 (2005)

[52] Coman, C.D., Bassom, A.P.: On the wrinkling of a pres-stressed annular thin film in tension. Journal of the Mechanics and Phyics of Solids **55**, 1601–1617 (2007)

[53] Coman, C.D., Haughton, D.M.: Localized wrinkling instabilities in radially stretched annular thin films. Acta Mechanica **185**, 179–200 (2006)

[54] Coman, C.D.: Bifurcation instabilities in finite bending of circular cylindrical shells. International Journal of Engineering Science **119**, 249–264 (2017)

[55] Coman, C.D.: Tensile bifurcations in a truncated hemispherical thin elastic shell. Zeitschrift für Angewandte Mathematik und Physik **71:178** (2020)

[56] Coman, C.D., Bassom, A.P.: Wrinkling of pre-stressed annular thin films under azimuthal shearing. Mathematics and Mechanics of Solids **13**, 513–531 (2008)

[57] Coman, C.D., Bassom, A.P.: Singular perturbations and torsional wrinkling in a truncated hemispherical thin elastic shell. Journal of Elasticity **150**, 197–220 (2022)

[58] Coman, C.D.: Lateral buckling of drill strings revisited: localised snaking. Accepted for publication (2023)

[59] Coman, C.D., Bassom, A.P.: Asymptotic limits and wrinkling patterns in a pressurised shallow spherical cap. International Journal of Non-Linear Mechanics **81**, 8–18 (2016)

[60] Coman, C.D: Global asymptotic approximations for wrinkling of polar orthotropic annular plates in tension. International Journal of Solids and Structures **47**, 1572–1579 (2010)

[61] Nguyen, Q.C.: Stability and Nonlinear Solid Mechanics. John Wiley & Sons, Chichester (2000)

[62] Leipholz, H.: Stability of Elastic Systems. Sijthoff & Noordhoff, Alphen aan den Rijn (1980)

[63] Lin, Y.H., Wan, Y.M.: Asymptotic solutions of steadily spinning shallow shells of revolution under uniform pressure. International Journal of Solids and Structures **21**, 27–53 (1985)